Energy Proceedings
Vol 50, 2025
ISSN 2004-2965

Molecular simulation on H_2 adsorption in shale kerogen nanopores and implications for underground hydrogen storage

Fangtao Lyu [1, 2], Zhengfu Ning [1, 2*], Ying Kang [1, 2], Zejiang Jia [1, 2]

1 State Key Laboratory of Petroleum Resources and Prospecting, China University of Petroleum, Beijing 102249, China

2 Department of Petroleum Engineering, China University of Petroleum, Beijing 102249, China
(*Corresponding Author: ningzhengfu313@163.com)

ABSTRACT

Underground hydrogen storage (UHS) in shale reservoirs is increasingly recognized as a significant method for hydrogen storage, with H_2 adsorption on reservoir rocks playing a crucial role in this process. In this work, we utilized molecular simulation techniques to investigate the adsorption behavior of H_2 in the slit nanopores of shale organic kerogen and specifically analyzed the effects of gas pressure, pore size, reservoir temperature, and kerogen maturity on H_2 adsorption performance. The results indicate that H_2 forms a strong adsorption layer on the kerogen pore surfaces, and this layer density increases with rising pressure. The surface excess adsorption amount of H_2 increases initially with pressure and then decreases slowly after reaching a critical pressure. H_2 exhibits stronger adsorption performance in smaller pores, and higher temperatures are unfavorable for further H_2 adsorption. Due to the chemical composition differences among various types of kerogen, the H_2 adsorption capacity decreases with increasing maturity. However, the H_2 recovery efficiency remains above 90% under the same conditions. In practical applications of H_2 storage in shale reservoirs, it is advisable to prioritize strata with higher organic maturity. Additionally, it is essential to consider the impacts of reservoir pressure and temperature based on realistic conditions to select the most suitable reservoir depth for H_2 storage. This study reveals the gas adsorption phenomena involved in UHS at the molecular level, providing insights into the optimal selection of H_2 storage shale reservoirs.

Keywords: hydrogen storage, shale, kerogen, adsorption, molecular simulation

1. INTRODUCTION

With the continuous growth in global energy demand and the increasing emphasis on environmental protection, the development of clean energy and the application of efficient energy storage technologies have become major focal points in current scientific research[1, 2]. H_2 energy, with its high energy density, clean and pollution-free nature, and broad application prospects, is poised to become a vital component of future energy systems[3, 4]. However, the efficient storage and safe transportation of H_2 remain significant technical challenges that hinder its large-scale application. Therefore, finding an economical, efficient, and safe method for H_2 storage is an urgent necessity.

Shale gas, as a significant unconventional natural gas resource, is typically developed using horizontal drilling and hydraulic fracturing technologies[5-7]. However, as extraction continues, many shale gas wells gradually enter a depleted phase, significantly reducing their traditional economic value. Depleted shale gas reservoirs, with their abundant pore structures and complex fracture networks, offer potential advantages for H_2 storage. Storing H_2 in these depleted shale gas reservoirs not only enables effective UHS but also brings new economic and environmental benefits to decommissioned shale gas wells.

Kerogen, the primary source of oil and gas in shale formations, possesses several distinctive characteristics. Firstly, kerogen features a complex nanoporous structure[8], which serves as the storage space for hydrocarbons within the shale reservoir. Secondly, kerogen has a high specific surface area (SSA) and intricate pore structure, which endows it with a strong capacity to adsorb gas molecules[9]. These gas molecules can be adsorbed onto the surface and within the pores of kerogen through physical adsorption (van der Waals forces) and chemical adsorption (hydrogen bonding or covalent bonding). Consequently, organic kerogen, as an essential component of shale, has unparalleled advantages for H_2 storage. Molecular simulation methods, such as molecular dynamics (MD) simulations and Monte Carlo (MC) simulations, are currently crucial

This is a paper for the 16th International Conference on Applied Energy (ICAE2024), Sep. 1-5, 2024, Niigata, Japan.

tools for studying the mechanisms of UHS. These techniques can reveal the adsorption, diffusion, and permeation behaviors of H_2 in kerogen at the molecular level, helping researchers understand the impact of different pore structures and surface chemistries on H_2 storage performance. Raza et al.[10] utilized molecular simulation method to investigate the adsorption behavior of H_2 in kerogen matrices, finding that H_2 adsorption is influenced by temperature, pressure, kerogen type, and maturity. Chen et al.[11] employed MC simulations to explore the compositional distribution and phase behavior of H_2 and shale gas systems under multiscale conditions. Zhang et al.[12] used Grand Canonical Monte Carlo (GCMC) methods to compare H_2 adsorption behaviors in kerogen and montmorillonite nanopores, as well as the effects of cushion gases. Their results indicated that pure H_2 adsorption is stronger in kerogen than in montmorillonite, and cushion gases like CH_4 or CO_2 can reduce H_2 storage capacity through competitive adsorption. While previous studies have conducted molecular simulations to investigate H_2 adsorption and diffusion in organic and inorganic nanopores within shale, further exploration is needed to understand the effect of kerogen maturity on H_2 adsorption in kerogen slit nanopores.

In this study, we first established slit nanopore models of shale organic kerogen with varying maturities. Using a hybrid MC and MD approach, we investigated the adsorption behavior of H_2 within these kerogen pores. We focused on analyzing the effects of pressure, temperature, pore size, and kerogen maturity on H_2 adsorption performance from the perspectives of density distribution and surface excess adsorption. Finally, we offered insights into the practical application of UHS in shale reservoirs.

1.1 Model construction

In this study, the process of model construction for H_2 adsorption is illustrated in Fig. 1. Firstly, to build a kerogen matrix structure with density consistent with realistic shale reservoir conditions, we employed the Ar plate compression method. Different types of kerogen molecules were obtained from the study by Ungerer et al.[13]. As shown in Fig. 1(a), a fixed number of kerogen molecules were placed in an empty simulation box, with the box's length Lx set to 60 Å and width Ly set to 40 Å. Two Ar plates were positioned parallel to the top and bottom of the kerogen molecules. Initially, both top and bottom argon plates were fixed, allowing the kerogen molecules to undergo NVT relaxation at 900 K for 500 ps. Subsequently, the top Ar plate was unfixed while the bottom plate remained fixed. The top Ar plate was kept rigid, and a constant force F along the z-axis was applied to each Ar molecule in the plate to compress the kerogen molecules, and this force was calculated using Eq. (1). In the kerogen compression simulations, a pressure of 80 MPa, typical for deep shale reservoirs, was chosen, and compression simulations were conducted successively at temperatures of 900 K, 700 K, 500 K, and 323 K for 500 ps, with 323 K being the target reservoir temperature for this study. After kerogen compression, both top and bottom argon plates were fixed, and a 500 ps NVT relaxation at 323 K was performed to obtain a structurally relaxed kerogen matrix model, as shown in Fig. 1(b). To avoid the influence of Ar plates on the kerogen matrix structure, only repulsive interactions were considered between kerogen molecules and Ar plates during all simulation steps. Four kerogen matrix models were established, denoted as Type IIA-D, with kerogen molecule quantities of 10, 10, 12, and 20, resulting in kerogen matrix thicknesses H of 27.7, 26.1, 30.7, and 33.1 Å, respectively. Furthermore, two identical kerogen matrices were placed parallel to each other to form kerogen slit pores with a diameter D as the initial configuration for H_2 adsorption simulations, as shown in Fig. 1(c). All simulations were performed under the NVT ensemble, with temperature controlled by the Nose-Hoover thermostat with a timestep of 1 fs[14]. Periodic boundary conditions were applied in the x, y, and z directions during the simulation process.

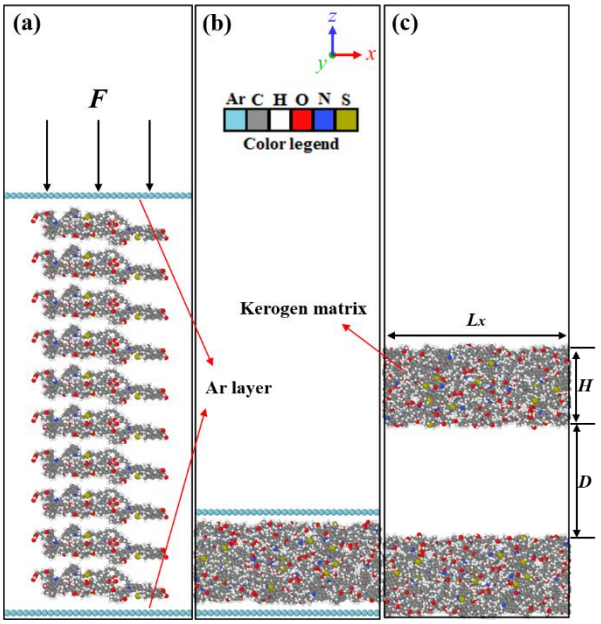

Fig. 1 Schematic diagram of the model construction process and related model parameters. (a) The initial configuration of kerogen compression; (b) The final configuration of kerogen compression; (c) The initial configuration of H_2 adsorption simulation.

$$F=\frac{pA_{xy}}{N} \quad (1)$$

where F is the constant force applied to each atom in the piston, p is the target pressure of the simulation, A_{xy} is the projected area of the piston in the xy plane, and N is the number of atoms in the piston.

1.2 Simulation details

H_2 adsorption in kerogen slit pores was computed using the GCMC method, which ensures that the gas in the nanopores is in chemical equilibrium with the bulk phase gas in an infinite reservoir. Initially, arbitrary chemical potentials were used as input parameters for GCMC simulations in an empty box. Upon reaching stability, the corresponding gas pressure at the given chemical potential was obtained. By varying the input chemical potential, the relationship between gas pressure and chemical potential was established, enabling the determination of the chemical potential at the target gas pressure, which served as input for the simulations. Therefore, the adsorption simulations employed a combined MC and MD approach under the μVT ensemble. Initially, MC simulations were used to insert or delete H_2 molecules, while the molecular movement was realized through MD to achieve both chemical and dynamic equilibrium of gas molecules in the model. 50000 MC cycles were performed under different simulation conditions, with the first 30,000 cycles dedicated to system equilibration and the subsequent 20,000 cycles for data sampling. The adsorption simulations were conducted under the NVT ensemble, with temperature controlled by the Nose-Hoover thermostat and a timestep of 1 fs. Periodic boundary conditions were applied in the x, y, and z directions, while the kerogen matrix remained fixed. The porous structure of the kerogen matrix allows H_2 molecules to enter its interior through gaps on its surface. However, we primarily focused on surface adsorption in the kerogen slit pores. Therefore, during data sampling and analysis, our attention was directed towards the portion of H_2 molecules within the primary slit pores.

In the model construction and gas adsorption simulations, kerogen molecules were described using the CVFF force field[15], while H_2 molecules were characterized using the three-point linear charge model proposed by Alavi et al.[16], which has shown excellent performance in studying H_2 surface adsorption. Non-bonded interactions between all particles consisted of short-range interactions and long-range electrostatic interactions, as shown in Eq. (2). The short-range force was calculated using the 12-6 Lennard-Jones (LJ 12-6) potential with a cutoff radius set to 1.2 nm[17], while the long-range electrostatic force was represented by the Coulomb potential, computed using the particle-particle particle-mesh (PPPM) integration method[18]. Interactions between different particles were described by the Lorentz-Berthelot (LB) mixing rule[19]. All simulations were performed using the large-scale atomic/molecular massively parallel simulator (LAMMPS) software package[20], with visualization and post-processing conducted using the OVITO software package[21]. The basic physical properties of H_2, such as bulk density, were obtained from the NIST Chemistry Webbook[22].

$$U_{ij}(r_{ij})=4\varepsilon_{ij}\left[\left(\frac{\sigma_{ij}}{r_{ij}}\right)^{12}-\left(\frac{\sigma_{ij}}{r_{ij}}\right)^{6}\right]+\frac{q_i q_j}{4\pi\varepsilon_0 r_{ij}} \quad (2)$$

where the subscripts i and j represent two unlike particles; ε and σ denote the LJ energy and size parameters, respectively; r_{ij} is the distance between particle i and j; q_i and q_j are the charges carried by particles i and j; and ε_0 is the vacuum permittivity.

2. THEORETICAL ANALYSIS

Through simulations, we can obtain the quantity of H_2 molecules loaded into the kerogen slit nanopores under different conditions. From this, we can calculate the surface excess adsorption of H_2, represented as:

$$\Gamma_{ex}=\frac{<N_{H_2}>/N_A-\rho_b V_p/M_{H_2}}{2S_A} \quad (3)$$

where $<N_{H_2}>$ is the ensemble-averaged number of H_2 molecules under specific conditions; N_A is Avogadro's constant; ρ_b is the bulk density of H_2; V_p is the effective pore volume; M_{H_2} is the molar mass of H_2; and S_A is the surface area of the kerogen pores.

In the practical application of H_2 storage in shale reservoirs, stronger adsorption of H_2 molecules by the reservoir rocks indicates a greater storage capacity for H_2. However, this also implies that during H_2 extraction, as reservoir pressure changes, it becomes increasingly difficult to extract H_2 from the reservoir. This can lead to the trapping of H_2 within the shale reservoir, potentially resulting in H_2 loss. Therefore, we introduce the concept of recovery efficiency, expressed as:

$$RE=\frac{<N_F>-<N_I>}{<N_I>}\times 100\% \quad (4)$$

where RE is the recovery efficiency; $<N_F>$ and $<N_I>$ represent the ensemble-averaged number of H_2 molecules under final and initial conditions, respectively, such as different reservoir pressure conditions.

3. RESULTS AND DISCUSSION

3.1 Isothermal adsorption of H_2

In this section, we investigated the isothermal adsorption of H_2 at 323 K under different pressure conditions within various types of kerogen pores. The adsorption configurations of H_2 at different pressures in 4 nm type IIA kerogen pores are shown in Fig. 2. For clarity, only the H_2 molecules present in the slit pores are displayed. It is evident that as the pressure increases, the H_2 density in the kerogen slit pores increases, forming an adsorption layer on the pore walls with a density higher than that at the pore center. To observe this change more intuitively, we plotted the 1D density distribution of H_2 along the z-axis in 4 nm different types of kerogen pores under various pressures, as shown in Fig. 3. Clearly, H_2 molecules form an adsorption layer with a density higher than the bulk phase density on the upper and lower surfaces of the kerogen pores, and this layer's density increases with pressure. Simultaneously, the free gas density near the pore center also increases with pressure and matches the bulk density under the corresponding temperature and pressure conditions. Additionally, the H_2 density at the pore walls is not zero, mainly because the pore surface is relatively rough, allowing H_2 molecules to enter the kerogen matrix through surface gaps. The H_2 density at the pore walls increases with the kerogen maturity (IIA < IIB < IIC < IID), indicating an increase in surface roughness. Furthermore, we plotted the 2D density distribution of H_2 at 30 MPa in different types of kerogen pores, as shown in Fig. 4. It is more intuitively evident that the adsorption gas density on the pore surface increases with the maturity of the kerogen, indicating enhanced H_2 adsorption performance. This also further reflects the increase in pore surface roughness with the maturity of the kerogen.

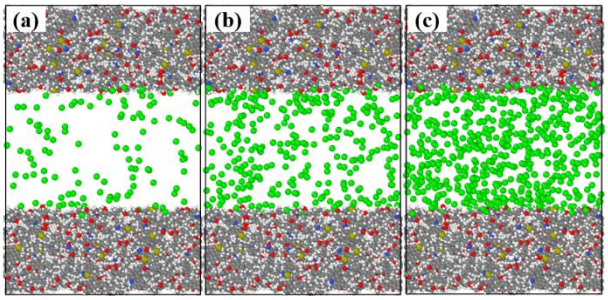

Fig. 2 Adsorption snapshots of H2 in 4 nm type IIA kerogen nanopores with the pressure of (a) 5 MPa, (b) 15 MPa and (c) 30 MPa at 323 K. For clarity, H_2 molecules are represented by green balls.

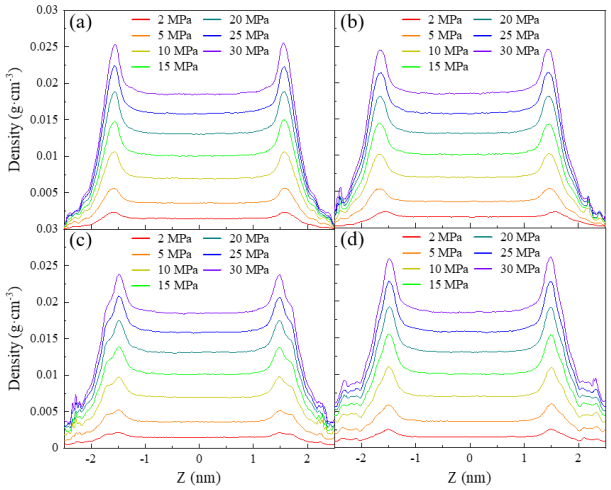

Fig. 3 1D density profiles of H_2 along the z-direction in 4 nm type (a) IIA, (b) IIB, (c) IIC, and (d) IID kerogen slit nanopores with various pressures at 323 K.

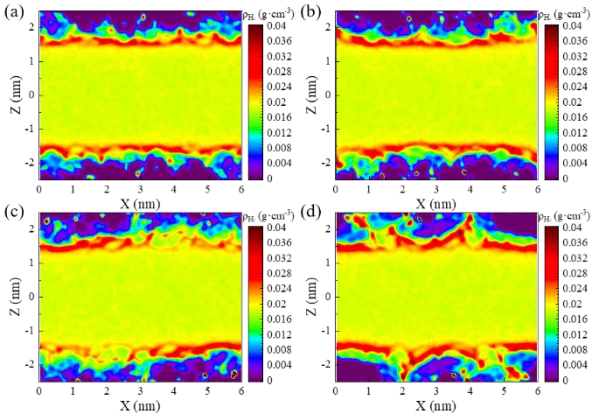

Fig. 4 2D density contour plots of H2 in 4 nm type (a) IIA, (b) IIB, (c) IIC, and (d) IID kerogen slit nanopores with a pressure of 30 MPa at 323 K.

Furthermore, based on the number of H_2 molecules loaded into kerogen slit pores under different conditions obtained from the simulations, we calculated the surface excess adsorption of H_2 in the pores. The adsorption isotherms of H_2 in different types of kerogen slit pores at 323 K are shown in Fig. 5. It can be observed that the surface excess adsorption of H_2 gradually increases with pressure, reaches a maximum, and then slowly decreases. The primary reason for this phenomenon is the continuous increase in the bulk density of H_2 with pressure. At relatively high pressures, the bulk density of H_2 increases significantly, resulting in a higher proportion of free gas in the pores. This leads to a reduction in the proportion of adsorbed gas, thereby decreasing the surface excess adsorption at high pressures. Additionally, the surface excess adsorption increases with the kerogen maturity, indicating that shale reservoirs with higher organic matter maturity have greater H_2 storage capacity. Therefore, for shale organic matter with well-

developed nanopores and larger SSA, the H_2 storage capacity is significantly enhanced.

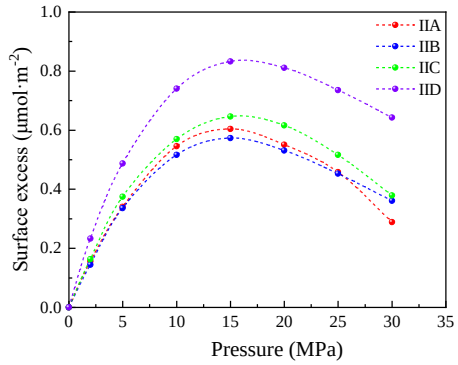

Fig. 5 Surface excess adsorption isotherms of H_2 in 4 nm different types of kerogen slit nanopores at 323 K.

In UHS projects, the capacity of shale reservoirs to store H_2 is crucial, and the further extraction of H_2 from these reservoirs is equally important for the effective utilization of the stored H_2. The recovery efficiency of H_2 in different types of kerogen pores, calculated according to Eq. 3, is shown in Fig. 6. This value represents the proportion of H_2 that can be extracted from the shale reservoir as the reservoir pressure continuously decreases until depletion during the extraction process. It can be seen that for the four types of kerogen pores with different maturities, over 90% of the H_2 can be extracted from the underground reservoir when the pressure drops from 30 MPa to 2 MPa. Although the recovery efficiency slightly decreases with the increasing maturity of the kerogen, due to its enhanced adsorption capacity for H_2, but the overall impact is not significant.

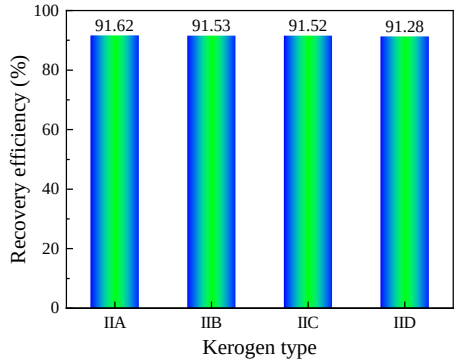

Fig. 6 Recovery efficiency of H_2 in 4 nm different types of kerogen slit nanopores at 323 K.

3.2 Effect of pore size on H_2 adsorption

Fig. 7 illustrates the surface excess adsorption of H_2 in kerogen pores of various sizes at 10 MPa and 323 K. For kerogen pores with different maturities, the surface excess adsorption of H_2 increases as the pore size decreases, indicating that smaller pores have a stronger gas adsorption capacity. This phenomenon primarily arises because, under the same temperature and pressure conditions, the proportion of adsorbed gas is higher in smaller pores. This makes shale reservoirs with highly developed nanopores a promising choice for H_2 storage. However, this does not imply that smaller pore sizes should always be pursued in UHS projects. While smaller pores exhibit stronger H_2 adsorption capabilities, they are limited by their own storage space, thereby restricting the total amount of H_2 that can be stored. Additionally, the higher proportion of adsorbed gas in smaller pores makes subsequent H_2 extraction more challenging, increasing the risk of H_2 loss. Therefore, in practical UHS applications, it is essential to balance these factors and select the most suitable operational strategies.

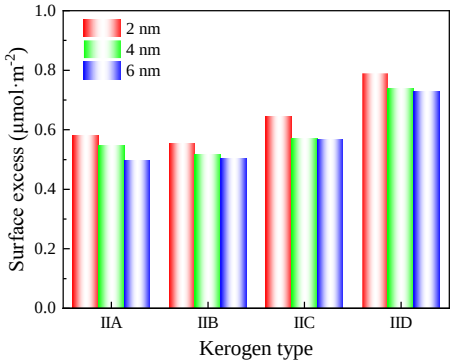

Fig. 7 Surface excess adsorption amount of H_2 in different types of kerogen slit nanopores with various pore sizes at 10 MPa and 323 K conditions.

3.3 Effect of temperature on H_2 adsorption

For shale reservoirs, the reservoir temperature increases with depth, rising from around 70~80°C in shallow to middle to over 120°C in deep reservoirs. This temperature variation significantly impacts the adsorption and storage of H_2. Fig. 8 shows the surface excess adsorption of H_2 in 4 nm different types of kerogen pores at 10 MPa as the temperature changes. It is evident that the surface excess adsorption of H_2 decreases with increasing temperature. This is primarily because H_2 adsorption on the kerogen pore surface is usually an exothermic process, mainly involving physical adsorption. When H_2 molecules move to the kerogen surface and get adsorbed, their kinetic energy reduces significantly, releasing heat (adsorption heat). Therefore, higher temperatures hinder further adsorption of H_2 molecules, resulting in a decrease in surface excess adsorption. Additionally, comparing H_2 adsorption in different types of kerogen pores under the same temperature and pressure conditions reveals that the surface excess adsorption of H_2 increases with kerogen maturity. From the above analysis, it can be inferred that the adsorption capacity of H_2 in shale reservoirs

decreases with increasing temperature (depth). However, the reservoir pressure generally increases with depth, which enhances H_2 adsorption capacity. Thus, in practical UHS projects, it is crucial to select the optimal depth or range for H_2 storage in advance.

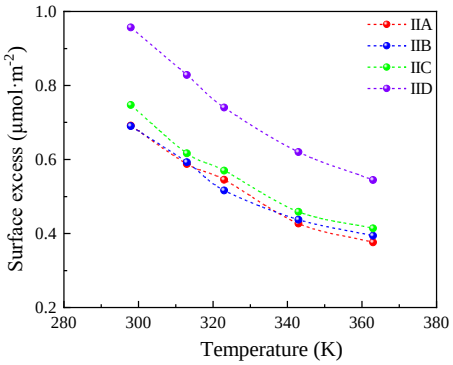

Fig. 8 Variation of surface excess adsorption amount of H_2 with temperature in 4 nm different types of kerogen slit nanopores at 10 MPa.

4. CONCLUSIONS

This study utilized molecular simulation method to investigate the adsorption behavior of H_2 in different types of shale organic matter kerogen nanopores and analyzed the effects of gas pressure, pore size, temperature, and kerogen maturity on H_2 adsorption capacity. The main conclusions obtained are as follows:

(1) H_2 adsorbs on the kerogen pore surface, forming a strong adsorption layer, and the density of this adsorption layer increases with increasing pressure. The surface excess adsorption of H_2 gradually increases with increasing pressure before slowly decreasing, but the overall apparent adsorption of H_2 in the pores continues to increase.

(2) The adsorption capacity of H_2 in kerogen pores increases with increasing kerogen maturity, while the recovery efficiency of H_2 shows a slight decrease, albeit remaining above 90%.

(3) H_2 exhibits stronger adsorption performance in smaller pores, and the adsorption of H_2 on the kerogen pore surface decreases with increasing temperature, mainly due to the exothermic nature of H_2 adsorption.

(4) In practical H_2 storage practices in shale reservoirs, reservoirs with higher organic matter maturity should be chosen. Additionally, the depth of the H_2 storage reservoir should be optimized, considering the beneficial effects of increasing pressure and the detrimental effects of rising temperature.

ACKNOWLEDGEMENT

This work was supported by the National Natural Science Foundation of China (Grant Nos. 51774298 and 51974330) and the Joint Funds of the National Natural Science Foundation of China (Grant No. U19B6003-03-04).

REFERENCE

[1] Tarhan C, Çil MA. A study on hydrogen, the clean energy of the future: Hydrogen storage methods. Journal of Energy Storage 2021;40:102676.

[2] Kittner N, Lill F, Kammen DM. Energy storage deployment and innovation for the clean energy transition. Nature Energy 2017;2(9):17125.

[3] Kovač A, Paranos M, Marciuš D. Hydrogen in energy transition: A review. International Journal of Hydrogen Energy 2021;46(16):10016-10035.

[4] Tashie-Lewis BC, Nnabuife SG. Hydrogen Production, Distribution, Storage and Power Conversion in a Hydrogen Economy - A Technology Review. Chemical Engineering Journal Advances 2021;8:100172.

[5] Yuan J, Luo D, Feng L. A review of the technical and economic evaluation techniques for shale gas development. Applied Energy 2015;148:49-65.

[6] Lyu F, Ning Z, Jia Z, Mu Z, Zhang W, Liu B. Investigation on gas/water two-phase flow in quartz nanopores from molecular perspectives. Journal of Molecular Liquids 2023;371:121145.

[7] Lyu F, Ning Z, Wu X, Wang Q, Gu K, Cheng Z, et al. A comparative study of gas transport in dry and moisturized shale matrix considering organic matter volume fraction and water distribution characteristics. Journal of Petroleum Science and Engineering 2022;208:109483.

[8] Bousige C, Ghimbeu CM, Vix-Guterl C, Pomerantz AE, Suleimenova A, Vaughan G, et al. Realistic molecular model of kerogen's nanostructure. Nature Materials 2016;15(5):576-582.

[9] Lyu F, Ning Z, Yang S, Mu Z, Cheng Z, Wang Z, et al. Molecular insights into supercritical methane sorption and self-diffusion in monospecific and composite nanopores of deep shale. Journal of Molecular Liquids 2022;359:119263.

[10] Raza A, Glatz G, Alafnan S, Mahmoud M, Gholami R. Depleted shale gas formations as naturally-occurring storage compartments for hydrogen: A molecular-level assessment. Fuel 2023;334:126695.

[11] Chen F, Mehana M, Nasrabadi H. Molecular Simulation of Hydrogen-Shale Gas System Phase Behavior under Multiscale Conditions: A Molecular-Level Analysis of Hydrogen Storage in Shale Gas Reservoirs. Energy & Fuels 2023;37(3):2449-2456.

[12] Zhang M, Yang Y, Pan B, Liu Z, Jin Z, Iglauer S. Molecular simulation on H2 adsorption in nanopores and

effects of cushion gas: Implications for underground hydrogen storage in shale reservoirs. Fuel 2024;361:130621.
[13] Ungerer P, Collell J, Yiannourakou M. Molecular Modeling of the Volumetric and Thermodynamic Properties of Kerogen: Influence of Organic Type and Maturity. Energy & Fuels 2015;29(1):91-105.
[14] Hoover WG. Canonical dynamics: Equilibrium phase-space distributions. Physical Review A 1985;31(3):1695-1697.
[15] Dauber-Osguthorpe P, Roberts VA, Osguthorpe DJ, Wolff J, Genest M, Hagler AT. Structure and energetics of ligand binding to proteins: Escherichia coli dihydrofolate reductase-trimethoprim, a drug-receptor system. Proteins: Structure, Function, and Bioinformatics 1988;4(1):31-47.
[16] Alavi S, Ripmeester JA, Klug DD. Molecular-dynamics study of structure II hydrogen clathrates. The Journal of Chemical Physics 2005;123(2):024507.
[17] Frenkel D, Smit B. Understanding molecular simulation: from algorithms to applications. Elsevier; 2001.
[18] Brown WM, Kohlmeyer A, Plimpton SJ, Tharrington AN. Implementing molecular dynamics on hybrid high performance computers – Particle–particle particle-mesh. Computer Physics Communications 2012;183(3):449-459.
[19] Lorentz HA. Ueber die Anwendung des Satzes vom Virial in der kinetischen Theorie der Gase. Annalen der Physik 1881;248:127-136.
[20] Plimpton S. Fast Parallel Algorithms for Short-Range Molecular Dynamics. Journal of Computational Physics 1995;117(1):1-19.
[21] Stukowski A. Visualization and analysis of atomistic simulation data with OVITO–the Open Visualization Tool. Modelling and Simulation in Materials Science and Engineering 2010;18(1):015012.
[22] Averill JD, Reneke P, Peacock RD. National Institute of Standards and Technology (NIST). 2004.